



Search for Pair Production of Doubly-charged Higgs Bosons in the $H^{++}H^{--} \rightarrow 4\mu$ Final State at DØ

The DØ Collaboration
URL <http://www-d0.fnal.gov>
(Dated: August 3, 2007)

A search for pair production of doubly-charged Higgs bosons via $p\bar{p} \rightarrow H^{++}H^{--} + X \rightarrow \mu^+\mu^+\mu^-\mu^- + X$ at $\sqrt{s} = 1.96$ TeV has been performed. We use a dataset corresponding to an integrated luminosity of about 1.1 fb^{-1} collected from April 19, 2002 to February 22, 2006 in Run II by the DØ detector of the Fermilab Tevatron Collider. Final states with at least three muons are considered. In the absence of a significant excess above the standard model background, 95% confidence level mass limits of $M(H_L^{\pm\pm}) > 150$ GeV and $M(H_R^{\pm\pm}) > 126.5$ GeV are set, respectively, for left-handed and right-handed doubly-charged Higgs bosons assuming a 100% branching ratio into muons.

Preliminary Results for Summer 2007 Conferences

I. INTRODUCTION

Doubly-charged Higgs bosons are predicted in many scenarios such as left-right symmetric models [1], Higgs triplet models [2] and little Higgs models [3]. At the Fermilab Tevatron Collider, there are two major production mechanisms. The first mechanism is pair production via $p\bar{p} \rightarrow Z/\gamma^* + X \rightarrow H^{++}H^{--} + X$. The leading-order diagram is shown in Fig.1. The second mechanism is single production via WW fusion, $p\bar{p} \rightarrow W^\pm W^\pm + X \rightarrow H^{\pm\pm} + X$. However, existing phenomenological and theoretical constraints can be easily satisfied if the $W^\pm W^\pm \rightarrow H^{\pm\pm}$ coupling is vanishing or very small [4]. Therefore, in this analysis only $H^{++}H^{--} + X$ production is considered. Depending on the $H^{\pm\pm}$ and H^\pm masses, the possible decay modes are $H^{\pm\pm} \rightarrow W^\pm W^\pm$, $H^{\pm\pm} \rightarrow W^\pm H^\pm$, $H^{\pm\pm} \rightarrow H^\pm H^\pm$ and $H^{\pm\pm} \rightarrow \ell^\pm \ell^\pm$, where H^\pm are singly-charged Higgs bosons and ℓ^\pm are charged leptons (e, μ, τ).

Since the H^{++} coupling to W pairs is suppressed due to the requirement that $\rho \equiv m_W^2 / \cos^2 \theta_W m_Z^2 = 1$ at tree level, the dominant final states are expected to be like-sign lepton pairs. The possible decay modes are decays in the e, μ and τ channel. Since these decays violate lepton flavor conservation, decay modes with mixed lepton flavor are also possible. Left-handed and right-handed states are distinguished by their decays into left-handed leptons or right-handed leptons.

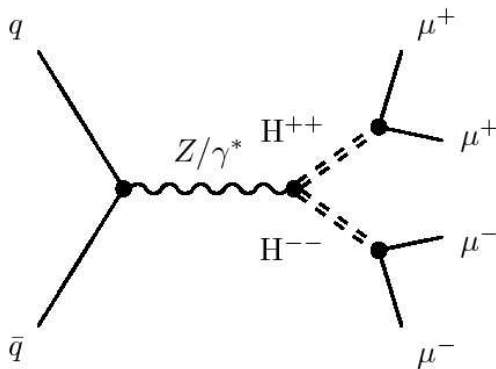


FIG. 1: Leading-order diagram for the pair production of doubly-charged Higgs bosons in $p\bar{p}$ collisions, where both Higgs bosons decay into muons.

Next-to-leading order (NLO) $H^{++}H^{--}$ pair production cross sections are shown in Fig. 2. The pair production cross section for left-handed doubly-charged Higgs bosons in the mass $100 < M(H^{\pm\pm}) < 200$ GeV is about a factor two larger than for the right-handed states due to different couplings to the intermediate Z boson [5].

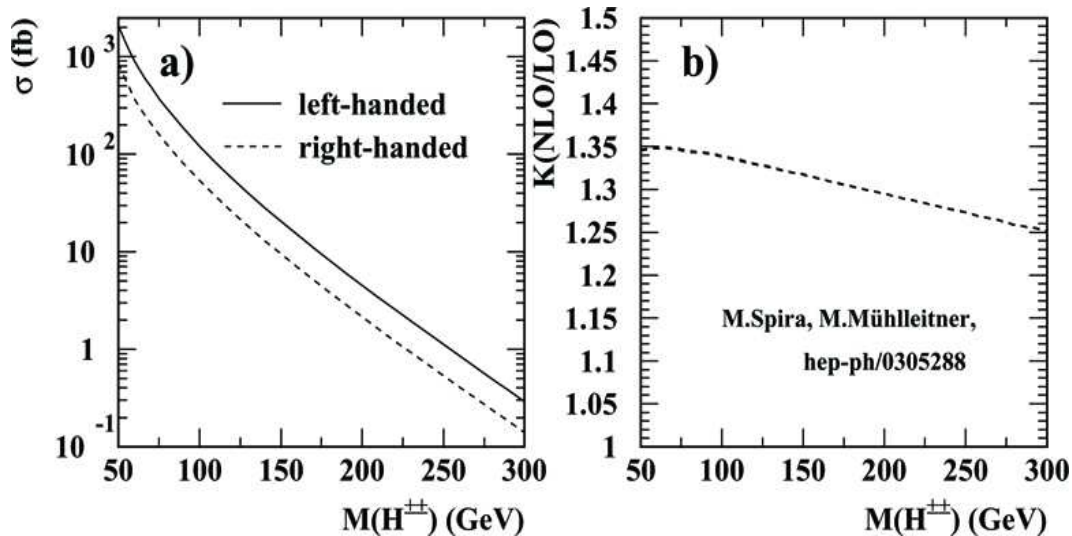


FIG. 2: a) NLO cross-sections and b) ratio of the NLO to LO cross-sections as a function of the mass of the doubly-charged Higgs boson, $M(H^{\pm\pm})$ [5].

Direct searches were performed by the OPAL, L3 and DELPHI collaborations at LEP in e^+e^- collisions. From

$e^+e^- \rightarrow H^{++}H^{--} \rightarrow 4\ell$ searches at LEP, doubly-charged Higgs bosons with masses below about 100 GeV have been excluded [6–8]. A previous search with 113 pb^{-1} data by the D0 collaboration in the $\mu\mu$ channel has excluded $H_L^{\pm\pm}$ below a mass of 118 GeV/c^2 and $H_R^{\pm\pm}$ below a mass of 98.2 GeV/c^2 [9]. With 240 pb^{-1} of $p\bar{p}$ collision data collected by the CDF II experiment a search for doubly-charged Higgs boson by the CDF collaboration in $\mu\mu$ channel has excluded $H_L^{\pm\pm}$ below a mass of 136 GeV/c^2 and $H_R^{\pm\pm}$ below a mass of 113 GeV/c^2 [10].

The main components of the D0 Run II detector important to this analysis are described briefly. The main detector systems include a magnetic central tracking system, a calorimeter and a muon detector [11].

The central tracking system consists of the silicon microstrip tracker (SMT) and the central fiber tracker (CFT) surrounded by a 2 T solenoidal magnet. The SMT has six barrel detectors, each with a set of four layers arranged axially around the beam pipe, and interspersed with 16 radial disks. The design is optimized for tracking and vertexing capability at $|\eta| < 3$. The CFT consists of scintillating fibers mounted on eight concentric cylinders. The fibers are constructed in ribbons each 128 fibers wide composed of two singlet layers. These singlet layers are formed into the ‘doublet’ layers which form the ribbon by placing the fiber of one of the singlet layers in the space between the fibers of the other singlet layer. The light from the fibers is converted into electrical pulses by visible light photon counters (VLPCs). They operate at temperatures from 6 to 15 Kelvin, which enables them to achieve a quantum efficiency (Q.E.) value well over 80%.

The calorimeter is a liquid argon sampling calorimeter. It is comprised of a central calorimeter (CC) covering a region up to a pseudo-rapidity of $|\eta| \approx 1.1$ and two end calorimeters (EC) extending the coverage to $|\eta| < 4.0$. The calorimeter is separated into an electromagnetic section (20 radiation lengths), a fine hadronic layer and a coarse hadronic layer.

Muon detector is composed of three main components: scintillators for triggering and cosmic rejection, a toroidal magnet to allow for an independent muon momentum measurement, and drift tubes to measure hit positions [12].

II. DATA SAMPLE

This analysis is based on the complete RunIIa data set collected with the D0 detector at the Fermilab Tevatron Collider from April 19, 2002 to February 22, 2006. Events are collected using all possible dimuon and single muon triggers. After data quality requirements, the total integrated luminosity of the sample is approximately 1.1 fb^{-1} .

III. MONTE CARLO SAMPLES

The standard model backgrounds and signal processes have been generated with PYTHIA 6.323. The $Z/\gamma \rightarrow ll$ cross section is calculated with CTEQ6L1 PDFs according to [13]. The $t\bar{t}$ cross section is calculated at NNLO in [14] and the WW , ZZ and WZ cross sections are calculated in [15] MCFM using CTEQ6L1 PDFs. All background Monte Carlo samples and cross sections used in this analysis are shown in Table I.

Process	Mass Range [GeV]	$\sigma \times \text{Br}$ [pb]
$Z/\gamma^* + X \rightarrow \mu\mu + X$	$15 < M < 60$	455 ± 16.8
$Z/\gamma^* + X \rightarrow \mu\mu + X$	$60 < M < 130$	242 ± 8.2
$Z/\gamma^* + X \rightarrow \mu\mu + X$	$130 < M < 250$	1.96 ± 0.6
$Z/\gamma^* + X \rightarrow \tau\tau + X$	$15 < M < 60$	455 ± 16.8
$Z/\gamma^* + X \rightarrow \tau\tau + X$	$60 < M < 130$	242 ± 8.2
$Z/\gamma^* + X \rightarrow \tau\tau + X$	$130 < M < 250$	1.96 ± 0.6
$t\bar{t} \rightarrow b\bar{b}l\bar{l}\nu\nu$		0.70 ± 0.04
$WW \rightarrow 2\ell + 2\nu$		1.08
$WZ \rightarrow 3\ell + \nu$		0.11
$ZZ \rightarrow 4\ell \text{ or } 2\ell + 2\nu$		0.07

TABLE I: Integrated luminosities corresponding to the number of generated events for all background Monte Carlo samples and cross sections used in this analysis.

Simulated muons are corrected by the difference between data and MC in reconstruction and isolation efficiencies. Trigger efficiency corrections are not applied to the Monte Carlo sample. Instead, the Monte Carlo samples are normalized to the data using the Z bosons in the data between 60 GeV to 130 GeV after requiring the preselection and isolation requirements (S1 and S2) which are defined in Section IV.

IV. EVENT SELECTION

In the previous analysis [9], two like-sign muons were required as a final state. In this analysis we require a third muon, which increases the sensitivity. The dominant backgrounds are real tri-muon events from WZ and ZZ decays and contributions from $Z \rightarrow \mu\mu$ and QCD background which is estimated from data.

Muons are selected using tracks in the central tracking detector in combination with patterns of hits in the wire chambers and scintillators in the muon system.

S1 Events are required to have at least two muons which pass the following selections:

- transverse momentum $p_T > 15$ GeV
- pseudorapidity $|\eta| < 2.0$
- matched to a track in the central tracker with at least five hits in the CFT layers and at least two hits in the SMT layers.
This requirement reduces the charge mis-identification probability [16] as well as background from badly reconstructed tracks.
- cosmic veto using timing criterion on the hits in the scintillator layers.
- invariant mass of at least one muon pair > 30 GeV

S2 To remove the QCD background coming mainly from muons originating from semi-leptonic b decays, isolation criteria based on the calorimeter and tracking information are applied. The isolation criteria are defined as follows. The sum of the transverse energies of the cells in a annular ring around the muon direction is required to be

$$\sum_{cell,i} E_T^i < 2.5 \text{ GeV, for } 0.1 < R < 0.4$$

where $R = \sqrt{\Delta\phi^2 + \Delta\eta^2}$. A similar condition is defined for the total transverse momentum of all tracks excluding the one matched to the muon in a cone of radius 0.5 centered around the muon,

$$\sum_{tracks,i} p_T^i < 2.5 \text{ GeV, for } R < 0.5$$

S3 To reject background from $Z \rightarrow \mu^+\mu^-$ and QCD events, the angle $\Delta\phi$ between at least two muons is required to be less than 2.5 radians, since two muons from Z decays are mostly back-to-back. This requirement rejects, in addition to $Z \rightarrow \mu^+\mu^-$ events, some of the remaining muons from the semi-leptonic decays of b quarks in jets that were not removed by the isolation requirement S2.

S4 Require at least two muons which fulfilled S1, S2 and S3 in the event to be of like-sign charge. This requirement is also used for the instrumental background calculations.

S5 Require a third muon. The third muon should satisfy the following selections:

- transverse momentum $p_T > 15$ GeV
- pseudorapidity $|\eta| < 2.0$
- matched to a track in the central tracker without requirements on the number of SMT and CFT hits.
- cosmic veto using timing criterion on the hits in the scintillator layers.
- isolation requirement (S2)

V. QCD BACKGROUND

The QCD background contribution is estimated directly from the data. All estimations of the QCD background are made after applying the preselection (S1). Differential distributions of QCD background are obtained by inverting the isolation requirement ($\sum_{cell,i} E_T^i \geq 2.5$ GeV and $\sum_{tracks,i} p_T^i \geq 2.5$ GeV) for both muons. $N_{data}^{\text{non-iso}}$ is defined as the number of the events in this selection: the number of events after preselection (S1) with the two muons not fulfilling the isolation criteria. We extrapolate the QCD estimate from the non-isolated region to the isolated

region of the phase space by applying a normalization factor f_{QCD} . The number of like-sign QCD events $N_{\text{QCD}}^{\pm\pm}$ is estimated from the excess of like-sign events $N_{\text{data}}^{\pm\pm}$ above the expected contribution $N_{\text{MC}}^{\pm\pm}$ from all standard model backgrounds: $N_{\text{QCD}}^{\pm\pm} = N_{\text{data}}^{\pm\pm} - N_{\text{MC}}^{\pm\pm}$. Here $N_{\text{data}}^{\pm\pm}$ and $N_{\text{MC}}^{\pm\pm}$ are defined as the number of data and MC events after the preselection (S1) in like-sign sample (S4), respectively. The normalization factor f_{QCD} for the QCD sample is obtained by taking the ratio of the number of like-sign QCD events to the number of non-isolated events in the like-sign sample ($N_{\text{data}}^{\text{non-iso},\pm\pm}$) at the preselection level (S1). The normalization factor f_{QCD} is defined as

$$f_{\text{QCD}} = \frac{N_{\text{data}}^{\pm\pm} - N_{\text{MC}}^{\pm\pm}}{N_{\text{data}}^{\text{non-iso},\pm\pm}} = \frac{N_{\text{QCD}}^{\pm\pm}}{N_{\text{data}}^{\text{non-iso},\pm\pm}} \quad (1)$$

The QCD background contribution at preselection level (S1) before applying the like-sign requirement (S4) is obtained by multiplying f_{QCD} to the number of non-isolated events in the unlike-sign sample, $N_{\text{data}}^{\text{non-iso},\pm\mp}$ without the like-sign requirement (S4):

$$N_{\text{QCD}}^{\pm\mp} = f_{\text{QCD}} \times N_{\text{data}}^{\text{non-iso},\pm\mp} \quad (2)$$

The isolation efficiency is obtained from the like-sign sample. Assuming that events remaining after subtracting Monte Carlo from data are all QCD events, the isolation efficiency for QCD is defined as

$$\epsilon_{\text{iso}} = \frac{N_{\text{data}}^{\text{iso},\pm\pm} - N_{\text{MC}}^{\text{iso},\pm\pm}}{N_{\text{data}}^{\pm\pm} - N_{\text{MC}}^{\pm\pm}} = (8.25 \pm 0.7)\% \quad (3)$$

where $N_{\text{data}}^{\text{iso},\pm\pm}$ and $N_{\text{MC}}^{\text{iso},\pm\pm}$ are the number of data and MC events after the isolation requirement (S2) in like-sign sample (S4), respectively.

To get an estimation of the QCD contribution after applying the isolation requirement (S2), the isolation efficiency from QCD is multiplied to the QCD contribution. The number of events for this estimation is given in Table II.

TABLE II: The number of non-isolated and QCD events after each selection (S1 and S2). The first and second row correspond to events without and with like-sign requirement, respectively. The number of events in the second and third columns is the number of QCD events after preselection (S1) and isolation requirement (S2), respectively.

Selection	$N_{\text{data}}^{\text{non-iso}}$	$N_{\text{data}}^{\text{non-iso}} \times f_{\text{QCD}}$ $= N_{\text{QCD}}$	$N_{\text{data}}^{\text{non-iso}} \times f_{\text{QCD}} \times \epsilon_{\text{iso}}$ $= N_{\text{QCD}}^{\text{iso}}$
without like-sign	3334	5244	423
with like-sign (S4)	1206	1902	157

VI. CHARGE MIS-IDENTIFICATION PROBABILITY

There are two sources that cause charge to be mis-identified. The first source of charge mis-identification is due to the limited CFT acceptance at high η . Tracks in the region with CFT detector $|\eta| > 1.63$ have less than 16 CFT hits. The fewer hits a muon has, the more the charge of the muon tends to be mis-identified. The second source is from very high p_T tracks. The uncertainty on the measured curvature and a possible residual mis-alignment can cause a charge mis-identification.

Since the mis-identification of charge occurs mainly in $Z \rightarrow \mu\mu$ and the resulting mis-measured muon typically has high p_T , the dimuon mass above 70 GeV is used to measure the charge mis-identification probability. This selection also reduces the QCD background, since most QCD background events are peaked in the low mass range. The charge mis-identification rate is obtained by dividing the number of events in the selection with like-sign requirement (S1,S2 and S4) by the number of events without like-sign requirement (S1 and S2). The charge mis-identification rate is calculated for both data sample and $Z \rightarrow \mu\mu$ MC. In case of the measurement in data, backgrounds are subtracted from the data sample. The background includes all MC backgrounds and QCD contribution except $Z \rightarrow \mu\mu$ MC.

The dimuon invariant mass distributions for like-sign and without like-sign requirement for data and MC are shown in Fig.3. From these we compute

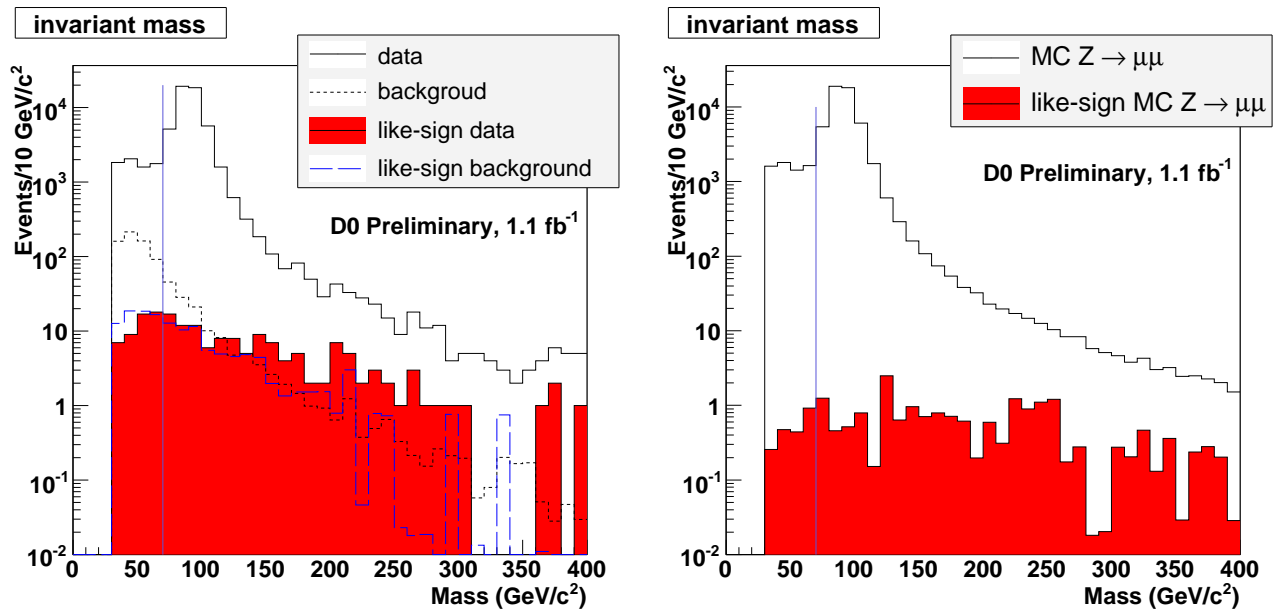


FIG. 3: The dimuon invariant mass distribution for data (left) and Monte Carlo $Z \rightarrow \mu\mu$ (right) events. The open and filled histograms correspond to the cases without and with like-sign requirement, respectively.

$$P_{\text{data}}^{\text{flip}} = (9.4 \pm 1.3) \times 10^{-4}$$

$$P_{\text{MC}}^{\text{flip}} = (3.90 \pm 0.9) \times 10^{-4}.$$

The uncertainties are statistical.

Since the charge mis-identification rate in the Monte Carlo simulation is underestimated, the ratio of the probability $P_{\text{data}}^{\text{flip}}$ from data to the $P_{Z \rightarrow \mu\mu \text{MC}}^{\text{flip}}$ from $Z \rightarrow \mu\mu$ MC is taken as a correction. The ratio k_{flip} is defined as

$$k_{\text{flip}} = \frac{P_{\text{data}}^{\text{flip}}}{P_{\text{MC}}^{\text{flip}}} = 2.41 \pm 0.67$$

The ratio is applied only to the $Z \rightarrow \mu\mu$ MC sample when estimating the like-sign contribution.

VII. COMPARISON OF DATA AND MONTE CARLO

The number of remaining events after each selection are shown in Table III. The distributions of dimuon invariant mass and $\Delta\phi$ are shown in Figs. 4–6. There is good agreement between data and the Monte Carlo simulation plus QCD, both in normalization and shape.

The third muon does not have any requirements on the number of SMT and CFT hits. However, if the third muon fulfills the CFT and SMT hit requirements in S1, then it is considered as a candidate muon in construction of a like-sign dimuon. In the events with more than one pair of muons that fulfills each of the selections, the invariant mass and $\Delta\phi$ between two muons are calculated only for the pair which has the muons with highest transverse momentum.

When the muons are required to be of like-sign charge most of the background from $Z \rightarrow \mu\mu$ are removed. The number of remaining events after each selection with like-sign requirement are shown in Table IV. This shows that the like-sign backgrounds are well understood.

In Figs. 4–6, the distribution of a left-handed doubly-charged Higgs signal with a mass $M(H^{\pm\pm}) = 140\text{GeV}$ are shown, with the normalization given by the NLO cross section, taking into account the experimental efficiencies. The number of expected signal events after each selection is shown in Table V for different masses. Total signal efficiencies lie in the range 30%–35%, and are nearly independent of mass.

A. High mass region

This study includes the region of dimuon invariant mass $M_{\mu\mu} > 200$ GeV. In the dimuon invariant mass plots (Fig. 4) a discrepancy is observed in this region.

The plots in Fig.7 indicates the following properties achieved in this region. It is well known that the mis-identified tracks are typically assigned much higher transverse momenta than the p_T it has been generated with. The leading muon is more vulnerable to mis-reconstruction than the second muon for the uncertainty on the measured curvature. Therefore the leading muon p_T has an excess over the high p_T region. A mis-reconstructed leading muon generates large missing E_T in the opposite direction of leading muon. Since the p_T of the second muon peaks around 40 GeV, it is conceivable to conclude that this discrepancy may be arising from Z decays where one of the decay muons is reconstructed badly.

To check this hypothesis, a further investigation is made by adjusting the leading p_T such that the missing E_T is 0 GeV. The leading p_T is modified by subtracting missing E_T since most of missing E_T comes from leading muon p_T . When the adjusted p_T is used to reconstruct an invariant mass, a peak at the Z mass is clearly observed as shown in Fig. 8.

Note that this effect in the data is not taken into account completely for the unlike-sign sample, while for the like-sign sample, it is taken into account by the charge mis-identification rate correction factor.

The $\Delta\phi$ requirement (S3) has been designed to remove such remaining Z boson decays responsible for the observed discrepancy.

TABLE III: The expected number of Monte Carlo background and QCD events and number of observed events after each selection. The simulation of Z decays includes the Drell-Yan contribution. Only statistical uncertainties are given in the Table.

Selection	Preselection S1	Isolation S2	$\Delta\phi < 2.5$ S3	Like sign S4	Third muon S5
Signal (140 GeV)	20.7	18.7	16.4	11.8	10.2
$Z \rightarrow \mu\mu$	69236	58325	4942	9.2	0.5 ± 0.4
QCD	5244	423	40.5	14.2	0.5 ± 0.2
$Z \rightarrow \tau\tau$	328	269	20.0	< 0.01	< 0.01
$t\bar{t}$	38	20	14	0.03	< 0.01
WW	40	34	20	< 0.01	< 0.01
WZ	19	16	11	3.0	1.6 ± 0.03
ZZ	11	9	5	0.6	0.5 ± 0.01
Total background	74917 ± 123	59096 ± 111	5052 ± 33	27 ± 1.7	3.1 ± 0.5
Data	74086	59347	4623	35	3
$S/\sqrt{S+B}$	0.08	0.08	0.23	1.89	2.79

TABLE IV: The expected number of events due to Monte Carlo backgrounds and QCD and number of observed events after each selection with like-sign requirement.

Selection (Like-sign)	Preselection S4 & S1	Isolation S2	$\Delta\phi < 2.5$ S3
Signal (140 GeV)	16.6	13.5	11.8
$Z \rightarrow \mu\mu$	115	59	9.2 ± 1
QCD	1902	157	14.2 ± 1
$Z \rightarrow \tau\tau$	3	0.2	< 0.01
$t\bar{t}$	7	0.04	0.03 ± 0.01
WW	0.08	0.04	< 0.01
WZ	5.2	4.3	3.0 ± 0.04
ZZ	1.1	0.9	0.6 ± 0.02
Total background	2033	221	27 ± 1.7
Data	1966	187	35

TABLE V: The number of expected signal events after each selection and efficiency for each mass point. The first row gives the number of expected events using the NLO cross section for left-handed $H^{\pm\pm}$ boson. The simulation is done in 10 GeV mass steps, but only every second mass point starting from 100 GeV is shown. The uncertainty of 1% is statistical.

M (GeV)	100	120	140	160	180	200
$N = \sigma L$	128	60	30	16	9	5
S1	87	40	21	11	6	3
S2	78	36	19	10	5	3
S3	67	32	16	9	6	3
S4	49	23	12	6	3	2
S5	42	20	10	5	3	2
ϵ ($\pm 1\%$)	33%	33%	34%	34%	33%	32%

VIII. CANDIDATE EVENTS

The run and event numbers as well as the invariant mass combinations between all muons in these events are given in Table VI and the kinematic properties of the individual muons in Table VII.

The largest remaining background after the third muon requirement is WZ background with 1.6 events. The contribution from $Z \rightarrow \mu\mu$ is 0.5 events. The expected QCD contribution is 0.5 events. Event (1) has large missing E_T . One muon from this event has no SMT hit. This muon could be mis-identified so that the p_T of the muon is changed. This event is therefore consistent with being a WZ event. Event (2) contains another not selected muon with a p_T of 12 GeV. This muon could come from a ZZ event. Event (3) has a muon which has $\eta > 1.6$. This could be the case of flipping charge from $Z \rightarrow \mu\mu + \text{jets}$.

	Run	Event	$M(\mu_1\mu_2)$	$M(\mu_1\mu_3)$	$M(\mu_2\mu_3)$	Missing E_T
(1)	175666	1137583	260.353 (++)	205.602 (--)	144.15 (+-)	138.20 GeV
(2)	203564	14775029	103.199 (+-)	86.3628 (+-)	67.1431 (--)	10.52 GeV
(3)	205114	3409480	124.463 (+-)	24.6714 (+-)	50.4876 (--)	43.72 GeV

TABLE VI: Run, event number and invariant masses of the three possible pairings of selected muons for the candidate events. Muons are numbered in descending p_T order. The charges of the muons are given in parentheses.

Muon	Charge	p_T (GeV)	η	ϕ	N_{SMT}	N_{CFT}	Quality
Event (1) Run 175666 event 1137583							
μ_1	-1	241.0	0.07	2.11	8	16	tight
μ_2	+1	40.0	-1.52	5.30	0	16	tight
μ_3	-1	31.9	1.37	4.59	3	16	tight
Event (2) Run 203564 event 14775029							
μ_1	+1	40.3	0.23	2.16	4	16	tight
μ_2	-1	39.7	-1.51	4.45	8	16	tight
μ_3	-1	35.7	-1.38	0.35	8	14	tight
Event (3) Run 205114 event 3409480							
μ_1	+1	36.9	-1.54	1.77	10	15	tight
μ_2	-1	17.2	1.61	5.99	8	15	tight
μ_3	-1	15.5	-0.57	1.55	8	16	tight

TABLE VII: Transverse momentum p_T , charge, pseudorapidity η , azimuthal angle ϕ and number of SMT and CFT hits for all muons in the candidate events. Event (2) contains another not selected tight muon which has momentum of 12.3 GeV.

IX. SYSTEMATIC UNCERTAINTIES

The following systematic uncertainties on signal and background are taken into account in the limit calculation. The systematic uncertainty on the luminosity is estimated to be 6.1% [17]. The systematic uncertainties on muon identification correction for backgrounds and signal are 2% and 6% respectively. The systematic error on the normalization

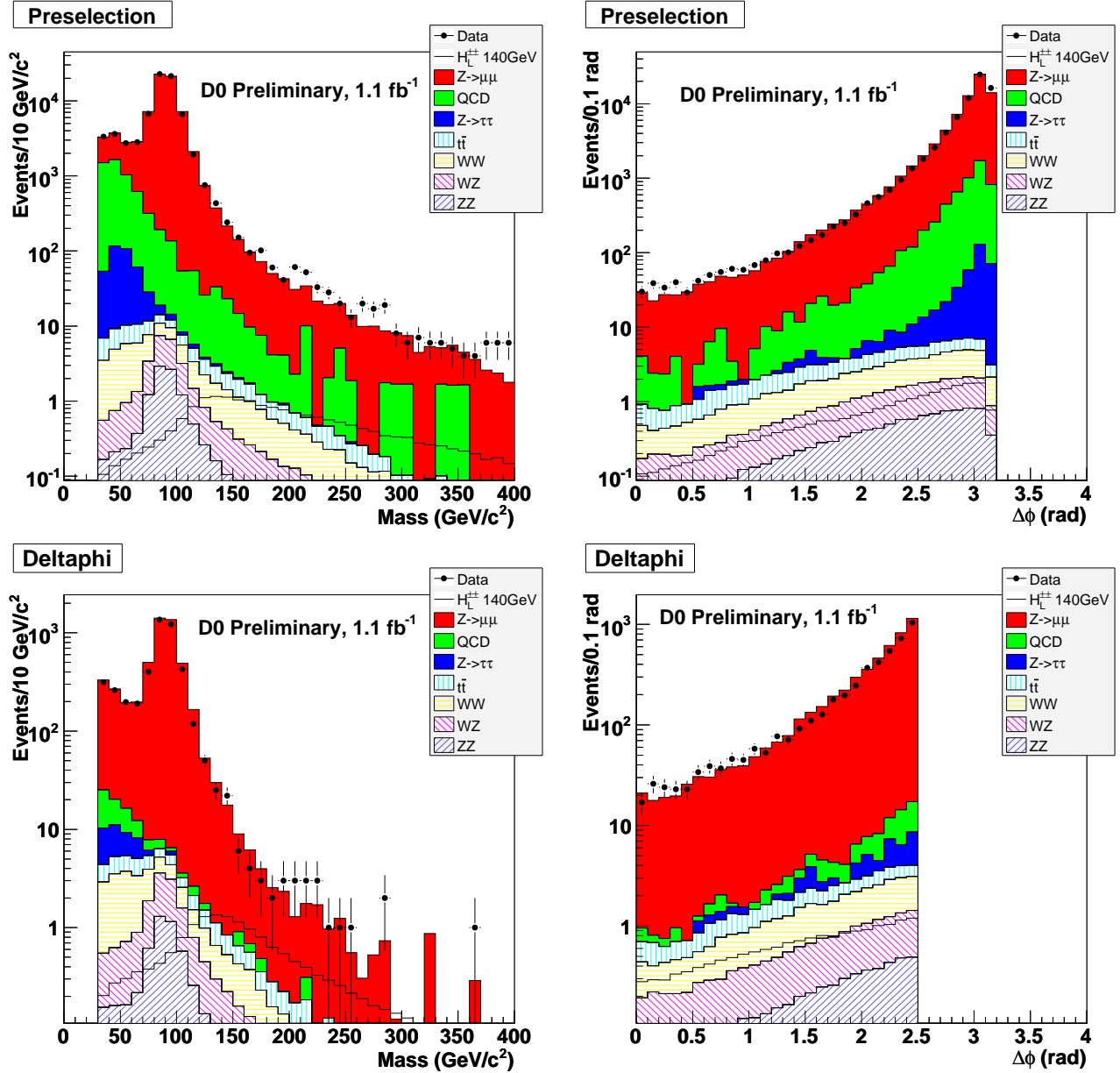


FIG. 4: Distribution of the dimuon invariant mass and $\Delta\phi$ between the two muons for data compared to the sum of Monte Carlo backgrounds after the preselection (S1) in upper plots and the $\Delta\phi$ requirement (S1-S3) in lower plots. Di-muon invariant mass and $\Delta\phi$ are calculated for the two highest p_T muons, independent of their charge. The signal expected for a left-handed $H^{\pm\pm}$, with $M(H^{\pm\pm}) = 140 \text{ GeV}/c^2$, is also shown by the open histogram.

using NNLO Monte Carlo background production cross sections is taken to be 5%. The theoretical uncertainty on the NLO $H^{\pm\pm}$ production cross section is about 10% [5]. The PDF uncertainties are less than 4%. The 27% uncertainty on the k_{flip} ratio applied to like-sign $Z \rightarrow \mu\mu$ is included. The uncertainty of 9% on the QCD isolation efficiency is also taken into account.

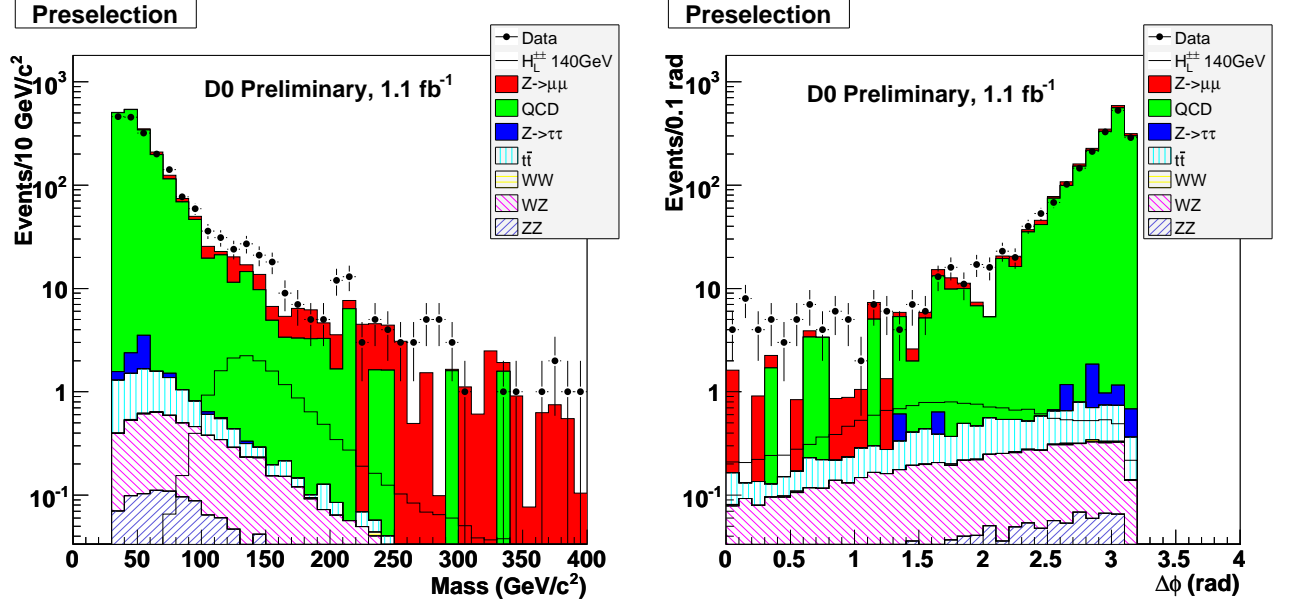


FIG. 5: Distribution of the dimuon invariant mass and $\Delta\phi$ between the two muons for data compared to the sum of Monte Carlo backgrounds after the preselection(S1) with the like-sign requirement(S4).

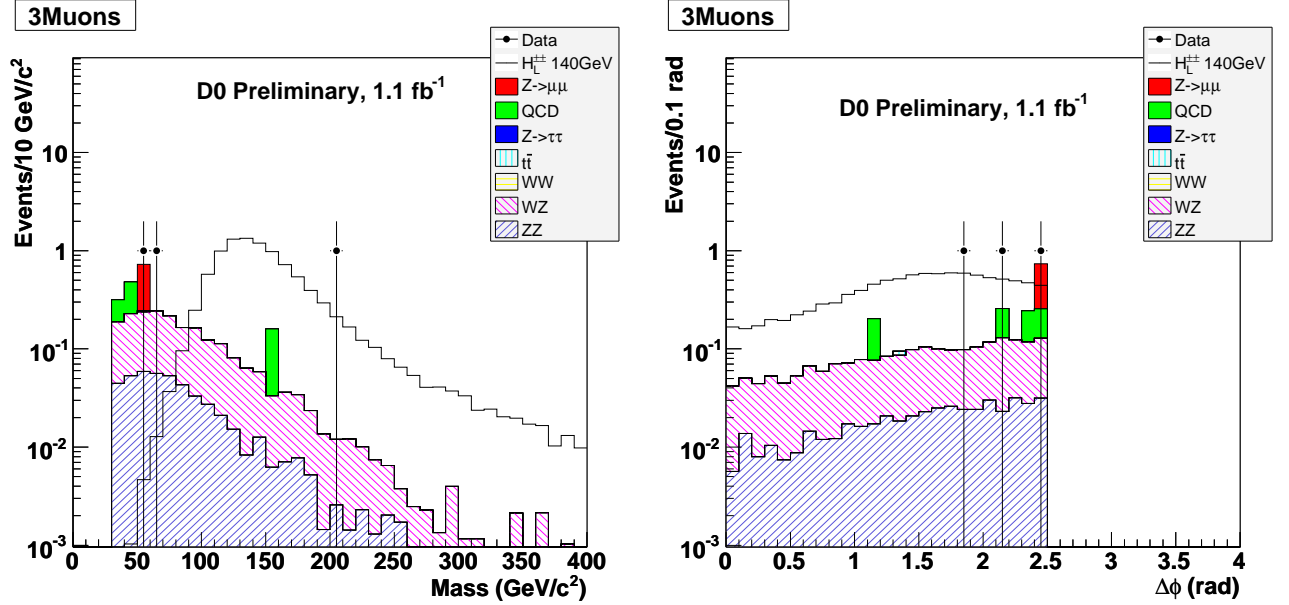


FIG. 6: Distribution of the dimuon invariant mass and $\Delta\phi$ between the two muons for data compared to the sum of Monte Carlo backgrounds after the third muon requirement (S1-S5).

X. RESULT

A search for $p\bar{p} \rightarrow H^{++}H^{--} + X \rightarrow \mu^+\mu^+\mu^-\mu^- + X$ has been performed. After full selection three data events remain, in good agreement with the standard model background expectation of 3.1 ± 0.5 events. Since no excess is observed, we proceed to set limits on the production cross-section times branching fraction using the CL_S method [18].

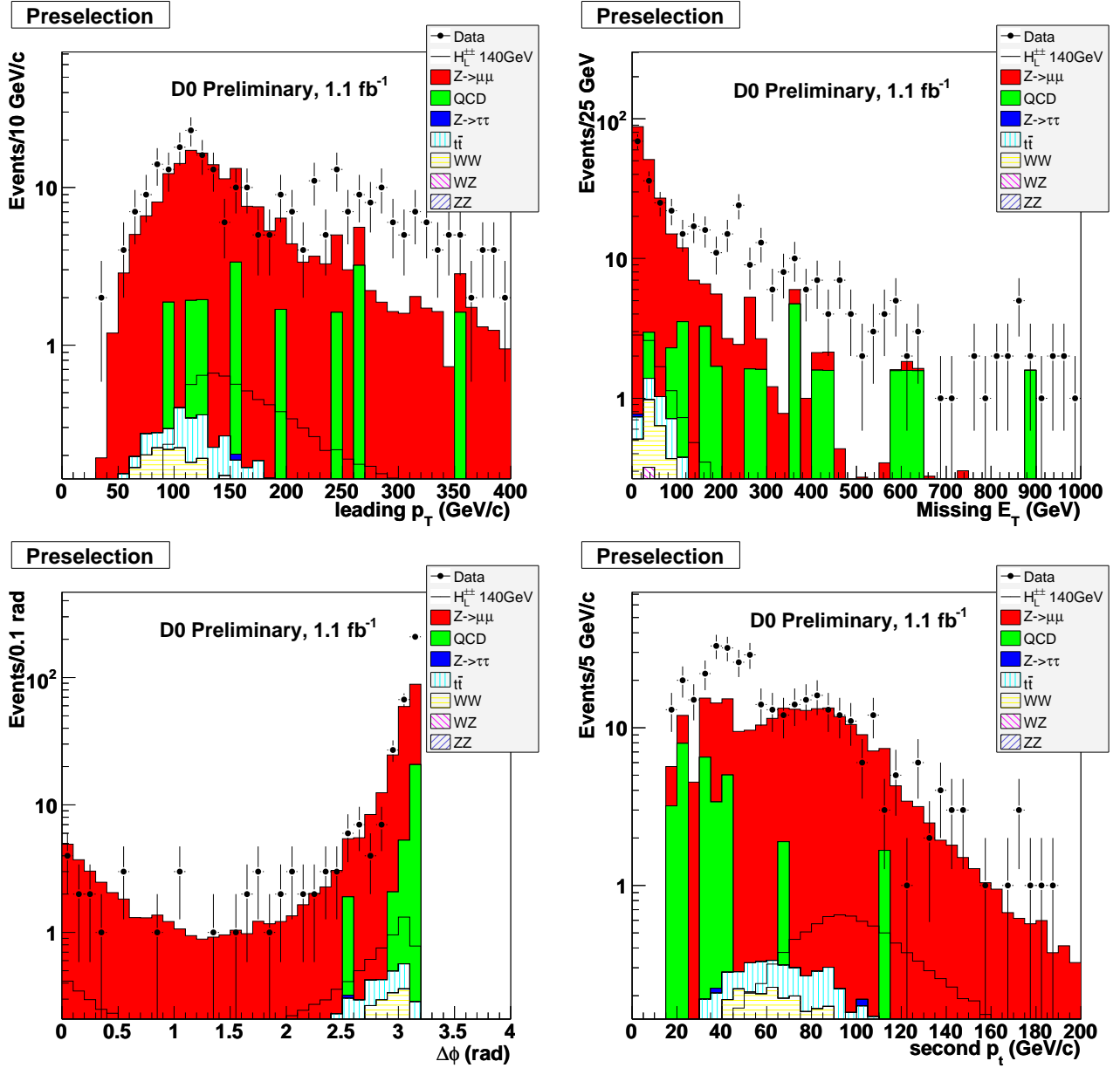


FIG. 7: (a) The excess of leading muon in the high p_T region in like- and unlike-sign dimuon data, (b) large missing E_T , (c) the direction between missing E_T and leading muon and (d) second muon peak around 40 GeV at Preselection level (S1) in the region of $M_{\mu\mu} > 200$ GeV.

We use the dimuon invariant mass distributions to calculate the confidence level. Statistical and systematic errors are considered. The limit calculation is performed using TLimit which has been adapted from the programs MCLIMIT [19]. The cross section limit as a function of the dimuon invariant mass is shown in Fig.9 together with the cross section of left- and right-handed doubly charged Higgs bosons from theory. At $CL_S=95\%$ a mass limit of 150 GeV for left-handed and a mass limit of 126.5 GeV for right-handed doubly-charged Higgs bosons is obtained. This significantly extends the current mass limits of $M(H_L^{\pm\pm}) > 136$ GeV for left-handed doubly-charged Higgs boson from the CDF collaboration.

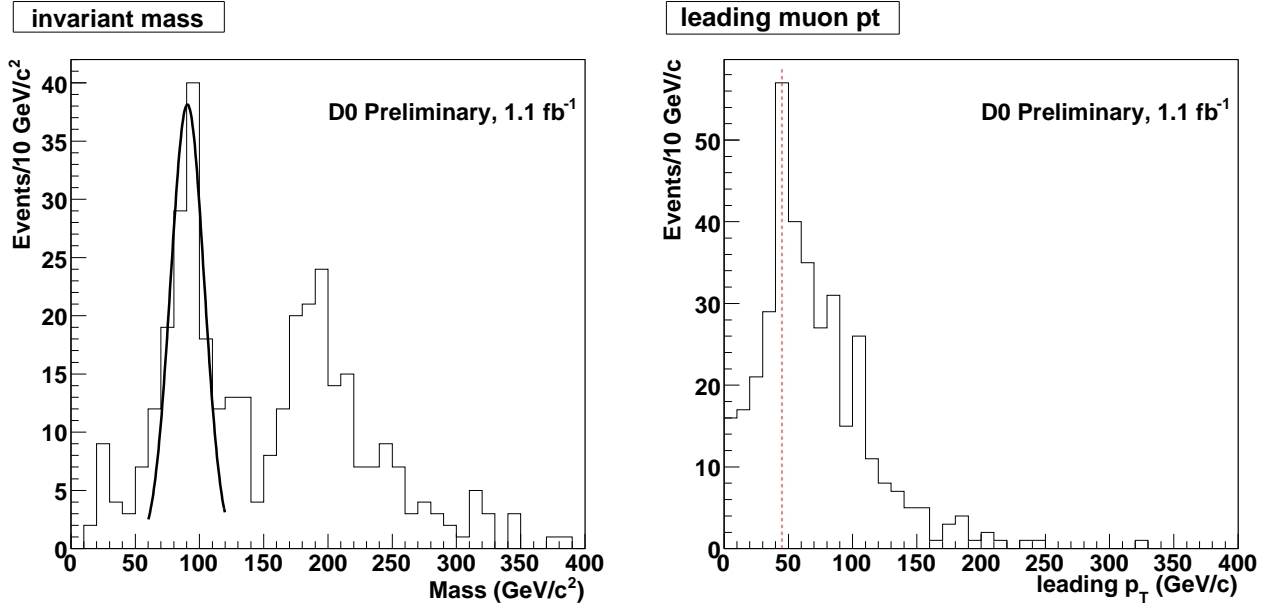


FIG. 8: The modified dimuon mass has a peak at Z boson mass (left plot). The gaussian function was used to fit the peak around 90GeV. The modified leading p_T now has a peak around 45 GeV (right plot).

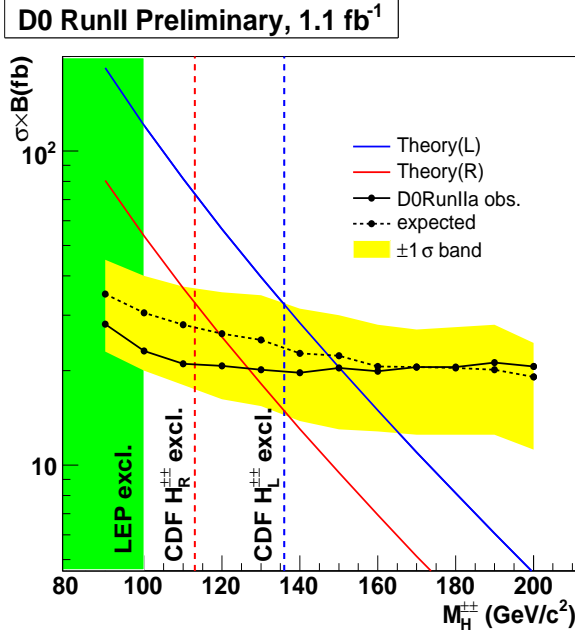


FIG. 9: The cross section limit as a function of the Higgs mass $M(H^{\pm\pm})$ at 95% confidence level. The $\pm 1\sigma$ uncertainty on the expected limit is given by the shaded area.

[1] N.G. Deshpande, J.F. Gunion, B. Kayser, Phys. Rev. D **44**, 837 (1991);
 J.F. Gunion, J. Grifols, A. Mendez, B. Kayser, and F. Olness, Phys. Rev. D **40**, 1546 (1989);
 T. Rizzo, Phys. Rev. D **25**, 1355 (1982) and Addendum-ibid D **27**, 657 (1983).
 [2] J.F. Gunion, C. Loomis, K.T. Pitts, hep-ph/9610237 (1996);

- J.F. Gunion, R. Vega, and J. Wudka, Phys. Rev. D **42**, 1673 (1990).
- [3] N. Arkani-Hamed et al., J. High Energy Phys. **0208**, 021 (2002).
 - [4] J.F. Gunion, H.E. Haber, G. Kane, S. Dawson, *The Higgs Hunter's Guide*, Frontiers in Physics.
 - [5] M. Mühlleitner, M. Spira, Phys. Rev. D **68**, 117701 (2003).
 - [6] OPAL Collaboration, G. Abbiendi et al., Phys. Lett. B **526**, 221 (2002);
OPAL Collaboration, P.D. Action et al., Phys. Lett. B **295**, 347 (1992).
 - [7] L3 Collaboration, P.Achard, Phys. Lett. B **576**, 18 (2003).
 - [8] DELPHI Collaboration, J. Abdallah et al., Phys. Lett. B **552**, 127 (2003).
 - [9] DØ Collaboration, Phys. Rev. Lett. **93**, 141801 (2004).
 - [10] CDF Collaboration, Phys. Rev. Lett. **93**, 221802 (2004).
 - [11] DØ Collaboration, V. Abazov et al., "The Upgraded D0 Detector", Nucl. Instrum. Methods, A **565**, 463 (2006).
 - [12] V. Abazov et al., "The Muon system of the RUN II D0 detector", Nucl. Instrum. Methods, A **552**, 372-398 (2005).
 - [13] R. Hamberg, W. L. van Neerven and T. Matsuura, Nucl. Phys. B **359**, 343 (1991) [Erratum-ibid. B **644**, 403 (2002)].
Program code available at <http://www.lorentz.leidenuniv.nl/~neerven>.
 - [14] N.Kidonakis, R. Vogt, hep-ph/0410367.
 - [15] http://www-clued0.fnal.gov/~nunne/cross-sections/mcgm_cross-sections.html.
 - [16] DØ Collaboration, hep-ex/0607032.
 - [17] T. Andeen et al., FERMILAB-TM-2365-E (2006).
 - [18] A. Read, J. Phys. G: Nucl. Part. Phys. **28**, 2693 (2002).
 - [19] T. Junk, Nucl. Instrum. and Methods, A **434**, 435 (1999).